BIOCHEMISTRY
including biophysical chemistry & molecular biology
Article

Biochemistry **2010,** *49,* 5841–5851 5841
DOI: 10.1021/bi100324z

Formation of the Complex of Nitrite with the Ferriheme *b* β-Barrel Proteins Nitrophorin 4 and Nitrophorin 7[†,‡]

Chunmao He, Hideaki Ogata, and Markus Knipp*

Max-Planck-Institut für Bioanorganische Chemie, Stiftstrasse 34-36, D-45470 Mülheim an der Ruhr, Germany

Received March 4, 2010; Revised Manuscript Received June 4, 2010

ABSTRACT: The interaction of ferriheme proteins with nitrite has recently attracted interest as a source for NO or other nitrogen oxides in mammalian physiology. However, met-hemoglobin (metHb), which was suggested as a key player in this process, does not convert nitrite unless small amounts of NO are added in parallel. We have recently reported that, in contrast, nitrophorins (NPs) convert nitrite as the sole substrate to form NO even at pH 7.5, which is an unprecedented case among ferrihemes [He, C., and Knipp, M. (2009) *J. Am. Chem. Soc. 131*, 12042−12043]. NPs, which comprise a class of unique heme *b* proteins from the saliva of the blood-sucking insect *Rhodnius prolixus*, appear in a number of concomitant isoproteins. Herein, the first spectroscopic characterization of the initial complexes of the two isoproteins NP4 and NP7 with nitrite is presented and compared to the data reported for metHb and met-myoglobin (metMb). Because upon nitrite binding, NPs, in contrast to metHb and metMb, continue to react with nitrite, resonance Raman spectroscopy and continuous wave electron paramagnetic resonance spectroscopy were applied to frozen samples. As a result, the existence of two six-coordinate ferriheme low-spin complexes was established. Furthermore, X-ray crystallography of NP4 crystals soaked with nitrite revealed the formation of an η^1-N nitro complex, which is in contrast to the η^1-O-bound nitrite in metMb and metHb. Stopped-flow kinetic experiments show that although the ligand dissociation constants of NP4 and NP7 (15−190 M^{-1}) are comparable to those of metHb and metMb, the rates of ligand binding and release are significantly slower. Moreover, not only the reaction kinetics but also electron paramagnetic resonance spectroscopy reveals notable differences between the two isoproteins

Nitrophorins (NPs)[1] comprise a unique class of ferriheme *b* proteins that are found in the saliva of the blood-sucking insect *Rhodnius prolixus* (*1*). From the saliva of these insects, four different NPs, designated NP1−4, have been isolated and characterized (*2*). Recently, a novel form, designated NP7, which is able to attach to negatively charged phospholipid membranes, was established by recombinant protein expression (*3*−*5*). The major biological function of these proteins is the delivery of NO to a host species during a blood meal.

Like many other heme proteins, NPs coordinate the heme iron by a His residue. The sixth coordination site of the iron is then ready to coordinate NO in the insect's saliva to be released upon administration to a host's tissue (*1*, *2*). In marked contrast to any other class of heme proteins, the protein fold consists mainly of β-strands, which form an eight-strand β-barrel that contains the cofactor; the fold is classified as a member of the lipocalin family (*6*). It was not until very recently that a heme *b* protein from *Arabidopsis thaliana* was described which consists of a 10-strand β-barrel (*7*). Previously, we have reported that NPs react with NO_2^- to form NO, where NO_2^- serves both as an electron donor and as an electron acceptor in a stoichiometry that is reflected by the total reaction depicted in Scheme 1 (*8*). This reaction is known as the nitrite disproportionation reaction that appears at low pH in aqueous solutions (*9*). However, NPs perform the reaction in a pH 7.5 buffered solution which has, to the best of our knowledge, not been reported for any other iron porphyrin.

Scheme 1

$$3NO_2^- + 2H^+ \xrightarrow{[NP^{III}]} 2NO + H_2O + NO_3^-$$

Another class of ferriheme *b* proteins that is currently being investigated for their interaction with NO_2^- consists of the globins, i.e., met-hemoglobin (metHb) (*10*) and met-myoglobin (metMb) (*11*). In the presence of small amounts of NO, a nitrite anhydrase/reductase reaction appears that may be of major importance for the physiological function of Hb via the production of N_2O_3 from blood NO_2^- (*12*−*15*). However, in the absence of NO, both metHb and metMb do not exhibit a reaction with NO_2^- other than NO_2^- binding (*16*).

Although some research has been conducted to elucidate the activation of NO_2^- by metMb, metHb, and several other ferriheme proteins, the exact mechanisms await adequate investigation. In case of the nitrophorins, this study is the first examination of the complex with NO_2^-, a prerequisite for understanding the mechanism of this unique reaction. For this purpose, UV−vis

[†]This work was financially supported by the Max Planck Society (MPG) and by the Deutsche Forschungsgemeinschaft (DFG), Grant KN 951/1-1 (to M.K.).

[‡]Coordinates and structure factor for the X-ray crystal structure of NP4 in a complex with nitrite reported here have been deposited in the Protein Data Bank (entry 3MVF).

*To whom correspondence should be addressed. Telephone: +49 (0)208 306 3581. Fax: +49 (0)208 306 3951. E-mail: mknipp@mpi-muelheim.mpg.de.

[1]Abbreviations: Hb, hemoglobin; HRP, horseradish peroxidase; HS, high-spin; ImH, imidazole; LS, low-spin; Mb, myoglobin; MALDI Q-TOF MS, matrix-assisted laser desorption ionization quadrupole time-of-flight mass spectrometry; metHb, ferriheme hemoglobin; metMb, ferriheme myoglobin; MOPS, 3-(*N*-morpholino)propanesulfonic acid; NiR, heme cd_1 nitrite reductase; NP, nitrophorin; py, pyridine; RR, resonance Raman; TpivPP, tetrakis(α,α,α,α-*o*-pivalamidophenyl)-porphyrinato dianion.

Published on Web 06/04/2010

absorption spectroscopy, electron paramagnetic resonance (EPR) spectroscopy, and resonance Raman (RR) spectroscopy were combined with stopped-flow kinetic measurements of both NP4 and NP7. Furthermore, X-ray crystallography of KNO_2-soaked NP4 crystals was performed. The data are discussed in comparison to those of other porphyrin[Fe^{III}—NO_2^-] complexes.

EXPERIMENTAL PROCEDURES

Materials. Stock solutions of $NaNO_2$ and KNO_2 were prepared freshly before use and the concentration was photometrically calibrated (ε_{210} = 5380 M^{-1} cm^{-1}) (*17*). All other reagents were of the highest grade commercially available and used as received.

NP4 and NP7 were recombinantly expressed in *Escherichia coli* strain BL21(DE3) (Novagen) and reconstituted as previously described (*4*, *18*). Protein preparations were routinely analyzed by SDS−PAGE to be >90% pure. The proteins were subjected to MALDI Q-TOF MS to confirm the correct molecular masses accounting for two Cys−Cys disulfides (calculated for $[NP4 + H]^+$ 20264 Da, observed 20279 Da; calculated for $[NP7 + H]^+$ 20969 Da, observed 20966 Da). Concentrations of NP4 and NP7 were determined photometrically using ε_{404} values of 141000 (*19*) and 81000 M^{-1} cm^{-1} (*4*), respectively. Human Hb was bought from Sigma. metHb was prepared by incubation with an excess of $K_3[Fe(CN)_6]$, followed by size-exclusion chromatography on Sephadex G-50. The concentration of metHb was determined photometrically using an ε_{405} of 180000 M^{-1} cm^{-1} (*16*).

Stopped-Flow Kinetic Measurements. The solvent of the protein was exchanged with 50 mM MOPS-NaOH (pH 7.0), and NP4 and NP7 were concentrated to 10 and 14 μM, respectively. Individually, reactant solutions of 200, 300, 400, 500, 600, and 800 mM $NaNO_2$ were prepared in 50 mM MOPS-NaOH (pH 7.0). To minimize mixing artifacts, NaCl was included in the protein solution at the same concentration as that of $NaNO_2$ in the respective reactant solution. The temperature of the solutions was equilibrated in the syringes of a water bath-thermostated UV−vis stopped-flow apparatus (RX.2000) equipped with a DA.1 pneumatic drive (Applied Photophysics Ltd.). The cuvette of the RX.2000 apparatus was inserted into the sample holder of a Cary 50 spectrophotometer (Varian Inc.). Upon temperature equilibration to 30 °C, the protein was mixed with the substrate while the absorption was followed at 404 nm. The absorbance was read every 0.1 s. The analysis of the kinetic data was performed using OriginPro version 7.5 (OriginLab Corp.).

Resonance Raman Spectroscopy. The solvent of the proteins was exchanged with 50 mM MOPS-NaOH (pH 7.0), and the concentration was adjusted to ~100 μM. For spectra of the NO_2^- complexes of metHb, NP4, and NP7, 200 mM $NaNO_2$ was added and the sample was incubated at room temperature for 5 min. The sample was quickly transferred to a 3 mm quartz tube and frozen in liquid N_2 where it was kept until measurement. RR spectra were recorded with a scanning double monochromator at 77 K. The excitation line at 413.1 nm was provided by a coherent K-2 Kr^+ ion laser.

EPR Spectroscopy. The solvent of the protein was exchanged with 50 mM MOPS-NaOH (pH 7.0), and the concentration was adjusted to ~100 μM. Upon being mixed with $NaNO_2$ at various concentrations, the sample was incubated at room temperature for a few minutes. The samples were quickly transferred into a 3 mm quartz tube and then rapidly frozen in liquid N_2 where they were kept until measurement. Continuous wave electron paramagnetic resonance (cw-EPR) spectra were recorded on a Bruker ESP-380E spectrometer at X-band equipped with a gas-flow cryogenic system with a liquid He cryostat from Oxford Inc. Spectra were recorded at 15 K with a microwave power of 2 mW, a field modulation of 100 kHz, and a modulation amplitude of 5 G. The obtained EPR spectra were simulated with the program GeeStrain5 version 1.0 (*20*).[2]

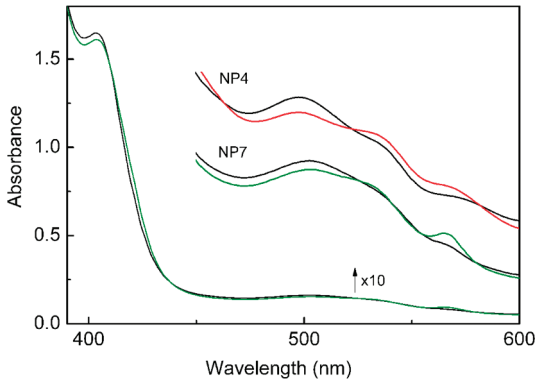

FIGURE 1: UV−vis absorption spectrum of 12 μM NP7 (green line) and 10 μM NP4 (red line) mixed with 50 mM $NaNO_2$ in 50 mM MOPS-NaOH (pH 7.0). For a comparison, the sums of the individual components are also displayed (black lines).

X-ray Crystallographic Analysis of the NP4−Nitrite Complex. Protein crystals were obtained using the vapor diffusion method with the conditions containing 3.2 M ammonium phosphate (pH 7.4). For the preparation of the nitrite complex, crystals were soaked in 3.2 M potassium phosphate (pH 7.4) with 15% glycerol and then in the same buffer supplemented with 0.2 M KNO_2 for 1 min. Afterward, the crystals were immediately frozen in liquid N_2 until the measurement. A diffraction data set was collected at 100 K using beamline BL14.2 at BESSYII (Berlin, Germany). The data sets were processed with XDS (*21*) and CCP4 (*22*). The molecular replacement method was applied to determine the phase using an initial model from NP4 [Protein Data Bank (PDB) entry 1X8Q]. Model building and refinement were conducted using Coot (*23*) and REFMAC5 (*22*), respectively. The stereochemical properties were checked by RamPage (*24*).

RESULTS

UV−Vis Absorption Spectroscopy of the Nitrite Complexes of NP4 and NP7. Unlike those of other heme proteins, the incubation of NPs with NO_2^- leads to the formation of NO in a pH 7.5 buffered solution according to Scheme 1 (*8*). This reaction is accompanied by the change in the Soret absorption maximum from 404 to 418 nm caused by the product, NO, which remains bound to the heme iron [$K_{eq}(NO) = 1.2 \times 10^{-7}$ M (NP4 at pH 8.0) (*25*), and $K_{eq}(NO) = 2.5 \times 10^{-7}$ M (NP7 at pH 7.5) (*5*)]. In the previous study, at 1 mM NO_2^-, the formation of the NP7[NO_2^-] complex was not observed in the absorption spectrum (*8*) because of the small $K_{eq}(NO_2^-)$ equilibrium constants (see below) in combination with the small absorption difference between NP and NP[NO_2^-]. As one can see in Figure 1, the addition of NO_2^- to a final concentration of 50 mM, which is significantly above $K_{eq}(NO_2^-)$ (see below), allows to record the UV−vis absorption spectra of NP4[NO_2^-] and NP7[NO_2^-] within 5 min upon incubation.

Besides the Soret band maximum at 404 nm, NP4 and NP7 show broad absorption maxima also at ~498 and ~503 nm,

[2]Available at http://www.bt.tudelft.nl/biomolecularEPRspectroscopy/.

respectively (*4*, *19*). A small band at ~530 nm originates from a fraction of the hydroxo complex.[3] As seen in Figure 1, the binding of excess NO_2^- to NP4 and NP7 leads to a slight red shift of the Soret band maximum to 406 nm with a relatively small decrease in the extinction coefficient [$\Delta\varepsilon_{404}(NO_2^-)$ = 3400 M^{-1} cm^{-1}]. The appearances of the α- and β-band are typical for the formation of low-spin complexes at 565 and 535 nm for NP4 and 567 and 533 nm for NP7, respectively. For metMb and metHb, the changes in the absorption spectrum upon NO_2^- binding were similar (*16*, *26*, *27*).

Determination of the Kinetic Parameters of the Nitrite Association Reaction of NP4 and NP7. Single-wavelength absorption detected (404 nm) stopped-flow kinetic measurements were performed with both NP4 and NP7, examples of which are shown in panels A and B of Figure 2. Experiments were performed in triplicate for a given NO_2^- concentration, and the results were averaged. However, it must be considered that the binding of NO_2^- to the NPs is only the initial step (see Scheme 2) of the total reaction represented by Scheme 1. For example, comparison of the rate constant for the formation of the NP[NO] complex at 30 °C with 300 mM NO_2^- versus that for the formation of the NP[NO_2^-] complex under the same conditions reveals that the formation of NO is significantly slower [$k_{obs}(NO) = 1.2 \times 10^{-3}$ s^{-1}, and $k_{obs}(NO_2^-) = 5 \times 10^{-2}$ s^{-1}] (see Figure S1 of the Supporting Information). On the other hand, the absorption change for the formation of NP[NO] is significantly larger than that for NP[NO_2^-] [$\Delta\varepsilon_{404}(NO) = 85800$ M^{-1} cm^{-1}]. Thus, the kinetic traces reflect the sum of NO_2^- binding and NO formation. Because NO formation during the recorded time is still in the linear initial phase, the last set of data points (3−5 min) were fit by linear regression analysis and the yielded function was subtracted from the kinetic trace before analysis with an exponential decay function (see Figure S2 of the Supporting Information).

The semilogarithmic plot of the data displayed in the insets of panels A and B of Figure 2 indicates that the data cannot be sufficiently approximated by a single exponential; however, a satisfying fit was obtained with a double exponential

$$A(t) = ae^{-tk} + be^{-tk'} + c \quad (1)$$

with A being the absorbance and t the time. In Figure 2C, the plot of k and k' for both NP4 and NP7 versus NO_2^- concentration is displayed, all of which reveal a linear behavior in agreement with a pseudo-first-order reaction. It should be mentioned that in case of the association reaction of NO with NP2 and NP3 a double exponential decay was applied (*25*, *28*) where the reaction among NP1, NP4, and NP7 was sufficiently described by a single-exponential fit (*5*, *25*). In the case of NP2 and NP3, a two-state model was used in which a NP2/3[NO] precomplex is expected to form in the first place (fast phase) followed by a monomolecular rearrangement toward the NP2/3[NO]* final complex (slow phase). The two-state model in this case is supported by the hyperbolic dependence of the slow phase on NO concentration (*28*). In contrast, the plots of k_{obs}^{slow} of NP4 and NP7 versus NO_2^- concentration show a linear dependence on NO_2^- concentration. Thus, the data were fit in accordance with Scheme 2 by the pseudo-first-order rate equation

$$k_{obs} = k_1[NO_2^-] + k_{-1} \quad (2)$$

[3]C. He and M. Knipp, work in progress.

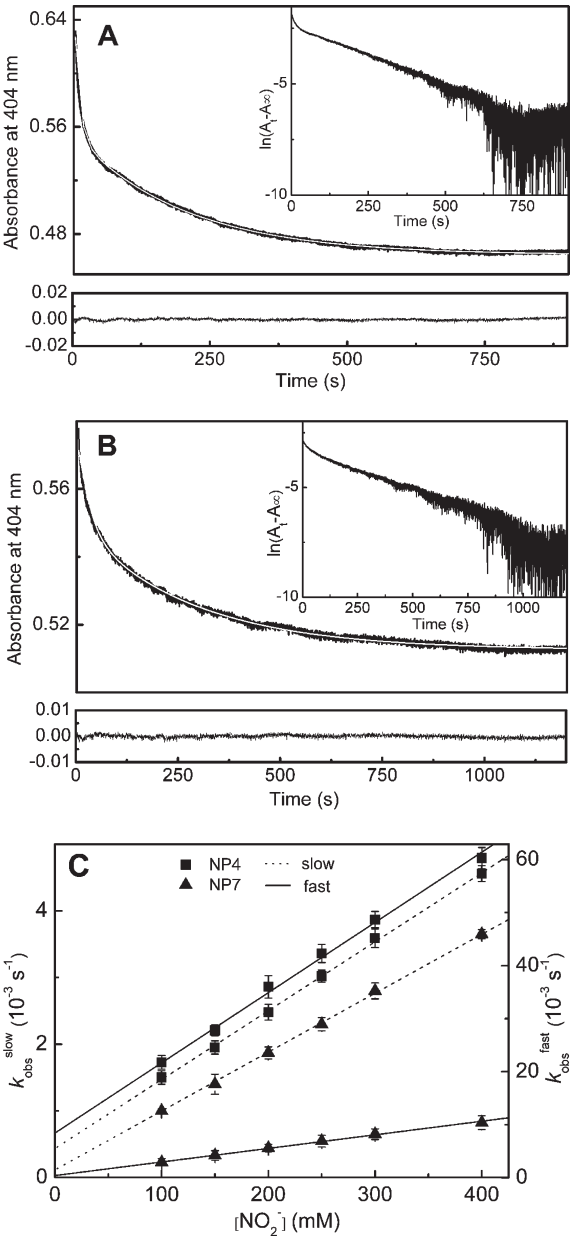

FIGURE 2: Representative examples of UV−vis absorption detected (404 nm) stopped-flow kinetics of the reaction between (A) NP4 (5 μM) or (B) NP7 (7 μM) and 300 mM $NaNO_2$ at pH 7.0 and 30 °C. The fit of the data by eq 1 is presented as a white line. The insets show a semilogarithmic representation of the data. (C) k_{obs} was plotted vs NO_2^- concentration, and data were fit with eq 2 [R^2 = 0.99862 (NP4, k_{obs}^{fast}), 0.99958 (NP4, k_{obs}^{slow}), 0.99899 (NP7, k_{obs}^{fast}), or 0.99992 (NP7, k_{obs}^{slow})].

Scheme 2

$$NP + NO_2^- \underset{k_{-1}}{\overset{k_1}{\rightleftharpoons}} NP[NO_2^-]$$

Such a behavior was previously described for metHb, and the data are interpreted as the appearance of a fast phase and a slow phase (see Discussion). The values are reported in Table 1 in comparison to reports for metHb and metMb. From these values, the equilibration constant

$$K_{eq} = \frac{k_1}{k_{-1}} \quad (3)$$

is estimated and reported in Table 1 as well.

Table 1: Rate Constants and Equilibrium Constants for the Binding of NO_2^- to NP4 and NP7 from *R. prolixus* in Comparison to metMb and metHb

	k_1^{fast} (M^{-1} s^{-1})	k_{-1}^{fast} (s^{-1})	k_1^{slow} (M^{-1} s^{-1})	k_{-1}^{slow} (s^{-1})	K_{eq} (M^{-1}) calculated fast[a]	K_{eq} (M^{-1}) calculated slow[b]	K_{eq} (M^{-1}) by titration	ref
NP4	0.13 ± 0.001[c]	0.0084 ± 0.0003[c]	0.01 ± 0.001[c]	0.00047 ± 0.00001[c]	15	21	178 ± 18[d]	tw[e]
NP7	0.076 ± 0.001[c]	0.00040 ± 0.00002[c]	0.0088 ± 0.0002[c]	0.00013 ± 0.00001[c]	190	68	400 ± 22[d]	tw[e]
metMb[f]	156 ± 3[g]	2.6 ± 0.1[g]	–	–	60	–	–	*16*
metHb[h]	260 ± 4[i]	1.70 ± 0.14[i]	28.1 ± 0.8[i]	0.20 ± 0.03[i]	153	141	–	*16*
metHb	–	–	–	–	–	–	556[j]	*30*
metHb[k]	–	–	–	–	–	–	901[l]	*26*
metHb[k]	–	–	–	–	–	–	333[l]	*27*
metHb[k]	140[m]	–	20[m]	–	–	–	–	*69*

[a] k_1^{fast}/k_{-1}^{fast}. [b] k_1^{slow}/k_{-1}^{slow}. [c] Performed at pH 7.0 and 30 °C. [d] Samples were prepared at ambient temperature and pH 7.0, and detection was performed by EPR spectroscopy at 15 K. [e] This work. [f] Horse Mb. [g] Performed at pH 7.4 and 20 °C. [h] Bovine Hb. [i] Performed at pH 7.4 and 30 °C. [j] Samples were prepared at ambient temperature and pH 7.4, and detection was performed by EPR spectroscopy at 77 K. [k] Human Hb. [l] Performed at pH 7.4 and 25 °C by optical titration. [m] Performed at pH 6.9 and 20 °C.

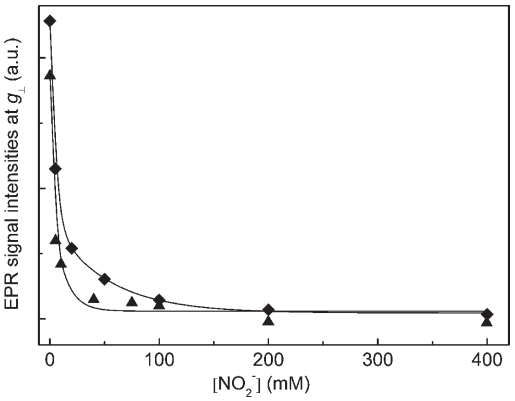

FIGURE 3: EPR signal intensities of (▲) NP7 and (◆) NP4 at $g_\perp$ (doubly integrated signal) vs NO_2^- concentration.

Determination of the Nitrite Association Constant of NP4 and NP7 by EPR Spectroscopy. According to the total reaction given in Scheme 1, the determination of $K_{eq}(NO_2^-)$ by simple titration experiments in solution under thermodynamic control, as is usually performed in studies of heme−ligand interactions (*29*), is not applicable. However, because cw-EPR spectroscopy allows the detection of the Fe^{III} high-spin species in frozen solutions, the signal intensity can be taken as a determinant of the degree of saturation with NO_2^-. For this purpose, samples of NP4 and NP7 were incubated with various concentrations of NO_2^- where equilibration was allowed for 5 min at ambient temperature. Afterward, the samples were rapidly frozen in liquid N_2 and kept frozen until the measurement. The optimum time for equilibration was estimated from a time-dependent experiment with both proteins in the presence of 200 mM NO_2^-. Samples were frozen after incubation for 2, 5, 10, and 20 min at room temperature (data not shown). Since the low-spin intensity for NP4 and NP7 slowly decreased after incubation for 5 min, i.e., the formation of NO reaches significant levels (compare Scheme 1), the system is equilibrated to the maximum possible extent.

For a comparison, the affinities of NO_2^- were also estimated by recording the EPR spectra of NP4 and NP7 incubated with various NO_2^- concentrations similar to what has been reported for metHb (*12*, *30*, *31*). The resulting plot of the EPR signal intensity at $g_\perp$ versus NO_2^- concentration [yielding $K_{eq(EPR)}^{NP4}(NO_2^-) = 178 \pm 18\ M^{-1}$ and $K_{eq(EPR)}^{NP7}(NO_2^-) = 400 \pm 20\ M^{-1}$] is displayed in Figure 3. As seen in Table 1, these values suggest

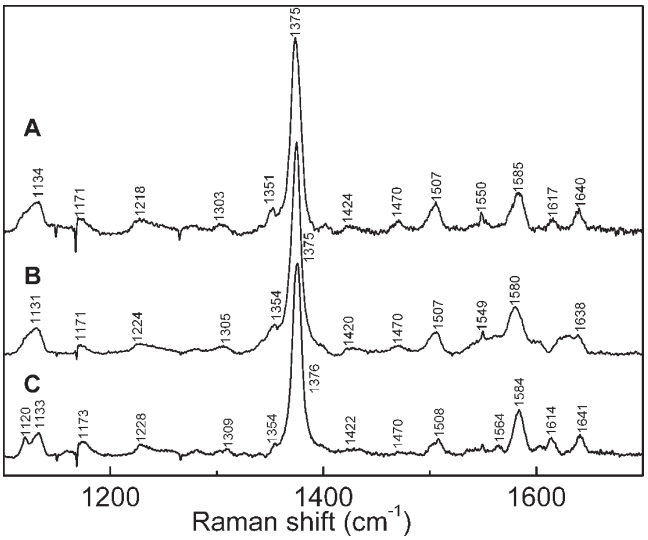

FIGURE 4: High-frequency RR spectra of (A) metHb[NO_2^-], (B) NP4[NO_2^-], and (C) NP7[NO_2^-] in 50 mM MOPS-NaOH (pH 7.0). Spectra were recorded at 77 K with a λ_{ex} of 413.1 nm.

a significantly higher NO_2^- affinity compared to the values obtained from the kinetic measurements, which is also true for metHb (*16*, *30*). However, unlike that for metHb (*27*), the thermodynamic equilibrium for the reaction displayed in Scheme 2 cannot be established because the reaction continues according to Scheme 1. Furthermore, it has to be considered that although the equilibration reaction can be performed at a defined temperature, the termination of the reaction and the sample preparation requires freezing; hence, before the sample reaches the frozen state, an undefined temperature decrease applies to the solution. Consequently, the obtained $K_{eq(EPR)}$ can only be considered as rough estimates for sample preparations in frozen solutions described in the following.

Resonance Raman Spectroscopy. RR spectra of NP4-[NO_2^-] and NP7[NO_2^-] together with a sample of metHb[NO_2^-] were recorded in frozen solution at 77 K, which allows the detection of the initial nitrite complex. To the best of our knowledge, this is the first published report of a RR study of ferriheme−nitrite adducts. All samples were excited into the Soret band absorption (see Figure 1) using a λ_{ex} of 413.1 nm. The resulting high-frequency spectra of NP4[NO_2^-], NP7[NO_2^-], and

Table 2: Comparison of the Raman Shifts (cm^{-1}) of the Aquo, NO, and NO_2^- Complexes of Ferriheme *b* Proteins NP1, NP4, and NP7 from *R. prolixus*, metMb from Horse Muscle, and metHb from Human Blood

protein	pH	temp (K)	ν_{10}	ν_2	ν_3	ν_4	ref
NP1	7.0	298	1611	1560	1481	1372	*32*
NP4	7.5	298	1610	1560	1481	1372	*35*
NP7	7.5	77	1615	1558	1484	1375	*8*
metMb	6.6	298	1611	1562	1482	1373	*34*
metHb	6.6	298	1610	1561	1481	1373	*34*
NP1[NO]	7.0	298	1636	1581	1504	1375	*32*
NP4[NO]	7.5	298	1640	1580	1505	1376	*35*
NP7[NO]	7.5	77	1640	1581	1509	1376	*8*
NP4[NO_2^-]	7.0	77	1638	1584	1507	1375	tw[a]
NP7[NO_2^-]	7.0	77	1641	1580	1506	1376	tw[a]
metHb[NO_2^-]	7.0	77	1640	1585	1507	1375	tw[a]

[a]This work.

metHb[NO_2^-] are depicted in Figure 4. The Raman shift frequencies of selected resonances with diagnostic potential for the assignment of the oxidation state and spin state are summarized in Table 2 in comparison to values of several ferric high-spin and nitrosyl ferric heme proteins from earlier reports.

For the nitrite complexes presented in Figure 4, the occurrence of the intense so-called oxidation state maker ν_4 = 1375 or 1376 cm^{-1} is typical for ferriheme proteins (*32*, *33*). This is also the case for the unliganded forms and NO complexes (Table 2). Another important feature seen in Figure 4 is the so-called spin state maker ν_3 that appears at 1507 or 1508 cm^{-1} which is diagnostic for six-coordinate low-spin (6cLS) hemes (1500−1510 cm^{-1}) (*34*). Where this also holds true for the nitrosyl complexes, the ν_3 resonance appears at 1480−1484 cm^{-1} in the case of the "unliganded" proteins, which is indicative of six-coordinate HS hemes (1475−1485 cm^{-1}) (*34*); i.e., the complexes have a water on them. Further, this spin state assignment is in good agreement with the Raman shifts of ν_{10} and ν_2 (*32*).

Overall, the RR spectra given in Figure 4 are highly similar. A significant difference can be seen in the region above 1600 cm^{-1}, where metHb[NO_2^-] and NP7[NO_2^-] exhibit clear bands at 1617 and 1614 cm^{-1}, respectively, whereas NP4[NO_2^-] exhibits an unresolved band in this region. The better resolution in the case of metHb and NP7 compared to NP4 holds true also for other ligand derivatives of these three proteins (*8*, *35*, *36*). For metMb, this resonance was assigned to the vinyl vibration $\nu_{(C=C)vinyl}$ (1621 cm^{-1}) (*36*) and hence indicates differences in the spatial environment of the heme substituents in NP4 compared to NP7.

In addition, in Figure 4, a well-separated band is seen at 1120 cm^{-1} for NP7[NO_2^-], which is not resolved in the case of metHb[NO_2^-] and NP4[NO_2^-]. On the basis of the previous attribution of this resonance in the case of deoxyMb (1117 cm^{-1}) and metMb[F^-] (1124 cm^{-1}), it can be assigned to the pyrrole C_b−vinyl stretch vibration (*36*). The lack of this band in Hb was previously noticed for metHb[F^-], although, and this is certainly also true for NP4[NO_2^-], the overlap with the neighboring band cannot be excluded (*36*). However, the band intensity is certainly weaker compared to those of NP7[NO_2^-] and metMb[F^-]. It was proposed that this resonance in Mb indicates an additional symmetry-lowering effect of the cofactor binding pocket, for example originating from charged groups, or dipoles, localized near the heme vinyls (*36*). In summary, besides the large spectral conformity depicted in Figure 4, subtle differences reflect the differences in the heme environment that may lead to variations in the ligand binding properties.

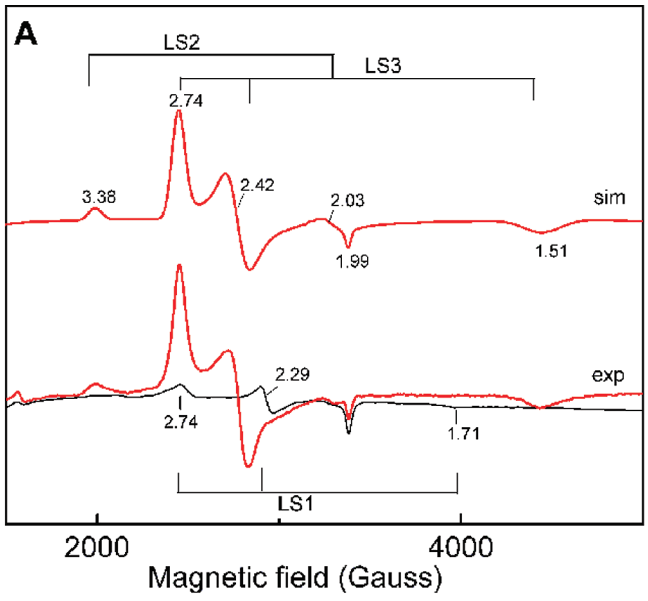

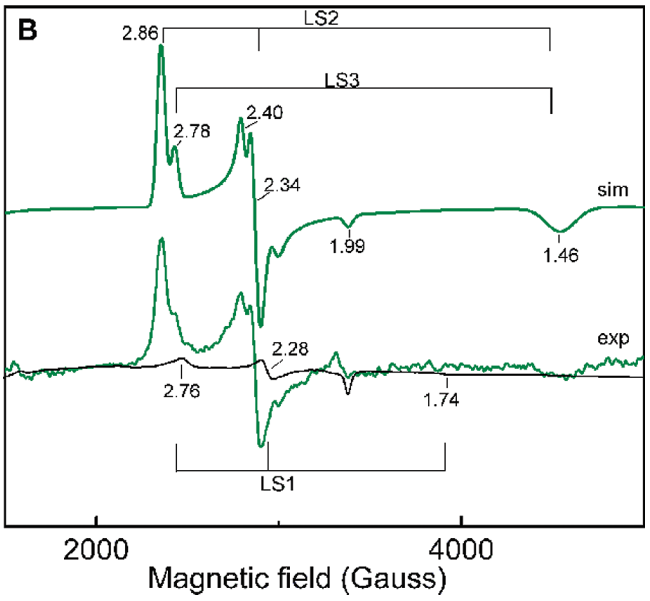

FIGURE 5: X-Band cw-EPR spectra of (A) NP4 and NP4[NO_2^-] and (B) NP7 and NP7[NO_2^-] recorded between 1500 and 5000 G. NP4 (200 μM) and NP7 (50 μM) were dissolved in 50 mM MOPS-NaOH (pH 7.0). For the spectra of the NP[NO_2^-] complexes, 200 mM $NaNO_2$ was added and samples were kept for 5 min at room temperature before being frozen. Spectra were recorded at 15 K. The corresponding *g* values are indicated in the spectra. Simulated spectra are designated "sim".

Characterization of the NP4 and NP7 Nitrite Complexes by cw-EPR Spectroscopy. The cw-EPR spectra of NP4 and NP7 frozen in a pH 7.0 buffered solution were recorded at 15 K and X-band frequency. An axial type of spectrum originating from the high-spin Fe^{III} form ($S = {}^5/_2$) of the proteins is detected with $g_\perp$ = 5.95 and $g_\parallel$ = 1.99 for NP4 and $g_\perp$ = 5.93 and $g_\parallel$ = 1.99 for NP7. These values are typical for most His-coordinated ferriheme *b* proteins with a water molecule bound to the iron, including metMb and metHb (*37*).

As one can see in Figure 5, a significant amount of a low-spin ($S = {}^1/_2$) rhombic type of spectrum (LS1) is also present in the

Table 3: Principle g Values of the Low-Spin Ferric Heme Complexes of NP4 and NP7 upon Binding of NO_2^- in Comparison to the EPR Parameters of Other Ferriheme[NO_2^-] Complexes

Fe^{III} porphyrin	reference or designation according to Figure 5	g_1	g_2	g_3	V/λ[a]	Δ/λ[b]	V/Δ	relative spin contribution[c] (%)
NP4[NO_2^-]	LS2	3.38	2.03	–	–	–	–	30
	LS3	2.74	2.42	1.51	2.26	2.17	1.04	70
NP7[NO_2^-]	LS2	2.86	2.34	1.46	1.95	2.55	0.76	80
	LS3	2.78	2.40	1.46	2.10	2.19	0.96	20
metHb[NO_2^-][d]	g values taken from ref *31*	3.03	2.33	1.47	1.77	2.91	0.61	nd[k]
		2.90	2.16	1.47	1.80	3.59	0.50	nd[k]
metHb[NO_2^-][e]	g values taken from ref *30*	2.98	2.12	1.41	1.63	3.66	0.44	nd[k]
		2.89	2.29	1.41	1.82	2.65	0.69	nd[k]
metMb[NO_2^-][f]	g values taken from ref *48*	3.11	2.30	1.00	1.27	1.94	0.66	40
		2.97	2.30	1.56	1.93	3.35	0.58	60
HRP[NO_2^-][g]	g values taken from ref *48*	2.99	2.24	1.31	1.58	2.67	0.59	–
NiR[NO_2^-][h]	g value taken from ref *48*	3.02	–	–	–	–	–	–
SiRHP[NO_2^-][i]	g values taken from ref *48*	2.93	–	–	–	–	–	50
		2.84	–	–	–	–	–	50
chlorite dismutase[NO_2^-][j]	g values taken from ref *70*	2.93	2.18	1.55	1.88	4.01	0.47	–
[Fe(TpivPP)(NO_2)(py)]	data taken from ref *42*	2.98	2.37	1.35	1.71	2.32	0.73	–
[Fe(TpivPP)(NO_2)(ImH)]	data taken from ref *42*	2.87	2.34	1.56	2.09	2.94	0.71	–

[a] $V/\lambda = g_x/(g_z + g_y) + g_y/(g_z - g_x)$. [b] $\Delta/\lambda = g_x/(g_z + g_y) + g_z/(g_y - g_x) - V/2\lambda$. [c] When obtained in the same EPR spectrum. [d] In a pH 6.5 buffered solution. [e] In a pH 7.4 buffered solution. [f] Sperm whale metMb at pH 7.7. [g] Horseradish peroxidase at pH 7.7. [h] *Thiobacillus denitrificans* heme cd_1 nitrite reductase at pH 7.7. [i] Heme protein subunit of the NADPH-sulfite oxidoreductase from *E. coli* at pH 7.7. [j] From the proteobacterium GR-1 at pH 7.0. [k] Not determined.

initial sample (for NP4, g = 2.74, 2.29, and 1.71; for NP7, g = 2.76, 2.28, and 1.74). These signals were assigned by pH titration experiments to originate from the hydroxide complexes.[3] Consequently, LS1 together with the high-spin signals disappears upon titration with NO_2^-.

Binding of NO_2^- to the iron center causes the appearance of two low-spin species, LS2 and LS3, in both NP4 and NP7. As one can see from the comparison with ferrihemes from literature in Table 3, the appearance of two low-spin species in ferriheme–NO_2^- complexes in proteins is a common phenomenon. The g values of $LS2^{NP7}$ and $LS3^{NP7}$ are very similar. They resemble a "normal" rhombic type of spectrum and, when compared to other ferriheme nitrite complexes, fit well in the range. Simulation of the spectra revealed $LS2^{NP7}$ to be the major species. The g values of $LS3^{NP4}$ are also very similar, in particular when compared to those of $LS3^{NP7}$, thus reflecting a comparable electronic situation. Remarkably, $LS2^{NP4}$ represents a "large g_{max}" spectrum with a g_{max} of 3.38 and is thus an exceptional case. However, spectral simulations reveal $LS3^{NP4}$ to be the major component (Table 3). From the resulting g values, the crystal field parameters Δ/λ (the tetragonality) and V/Δ (the rhombicity) were calculated according to the theory developed by Griffith and Taylor (*38*–*41*). For this purpose, the g values are assigned according to the "conventional" coordination system where $g_z = g_1$, $g_y = g_2$, and $g_z = g_3$. As a control, the orbital mixing parameters a, b, and c were calculated (*40*, *42*) to check how well the $a^2 + b^2 + c^2 \equiv 1$ relation is satisfied. Values between 0.99 and 1.02 were obtained in all cases, thus confirming the integrity of the g values.

X-ray Structure of the NP4–Nitrite Complex. Crystallization conditions for NP7 are not yet available. In contrast, crystallization conditions for NP4 are well established, and a number of ultra-high-resolution crystal structures were published (*43*). By analogy, crystals of NP4 were grown in ammonium phosphate (pH 7.4) (*44*), then soaked in potassium phosphate (pH 7.4) to remove the NH_3 ligand from the heme iron, and finally soaked in 200 mM KNO_2-containing buffer. The time for incubation with

Table 4: Data Collection and Refinement of the Data Sets of NP4 from *R. prolixus* Crystallized at pH 7.4 and Soaked with Nitrite[a]

	NP4[NO_2^-]
PDB entry	3MVF
Data Collection	
wavelength (Å)	0.91892
space group	*C*2
unit cell parameters	
a (Å)	70.31
b (Å)	42.91
c (Å)	52.46
β (deg)	94.05
resolution (Å)	30.53–1.40 (1.44–1.40)
no. of observed reflections	110960
no. of unique reflections	30694
R_{merge}	0.038 (0.193)
completeness (%)	97.7 (93.7)
$\langle I/\sigma(I)\rangle$	21.0 (6.8)
Refinement	
resolution range (Å)	15.0–1.4
R (%)	13.6
R_{free} (%)	18.7
no. of residues	184
no. of solvent molecules	223
no. of NO_2^- ions	2
rmsd[b] for bond lengths (Å)	0.025
rmsd[b] for bond angles (deg)	2.22
Ramachandran plot	
favored region (%)	99.5
allowed region (%)	0.5
outlier region (%)	0
average B factor (Å^2)	
protein	15.3
ligand (heme)	13.9
ligand (NO_2^-)	23.7
solvent	28.1

[a] Numbers in parentheses represent the values for the highest-resolution shell. [b] Root-mean-square deviation.

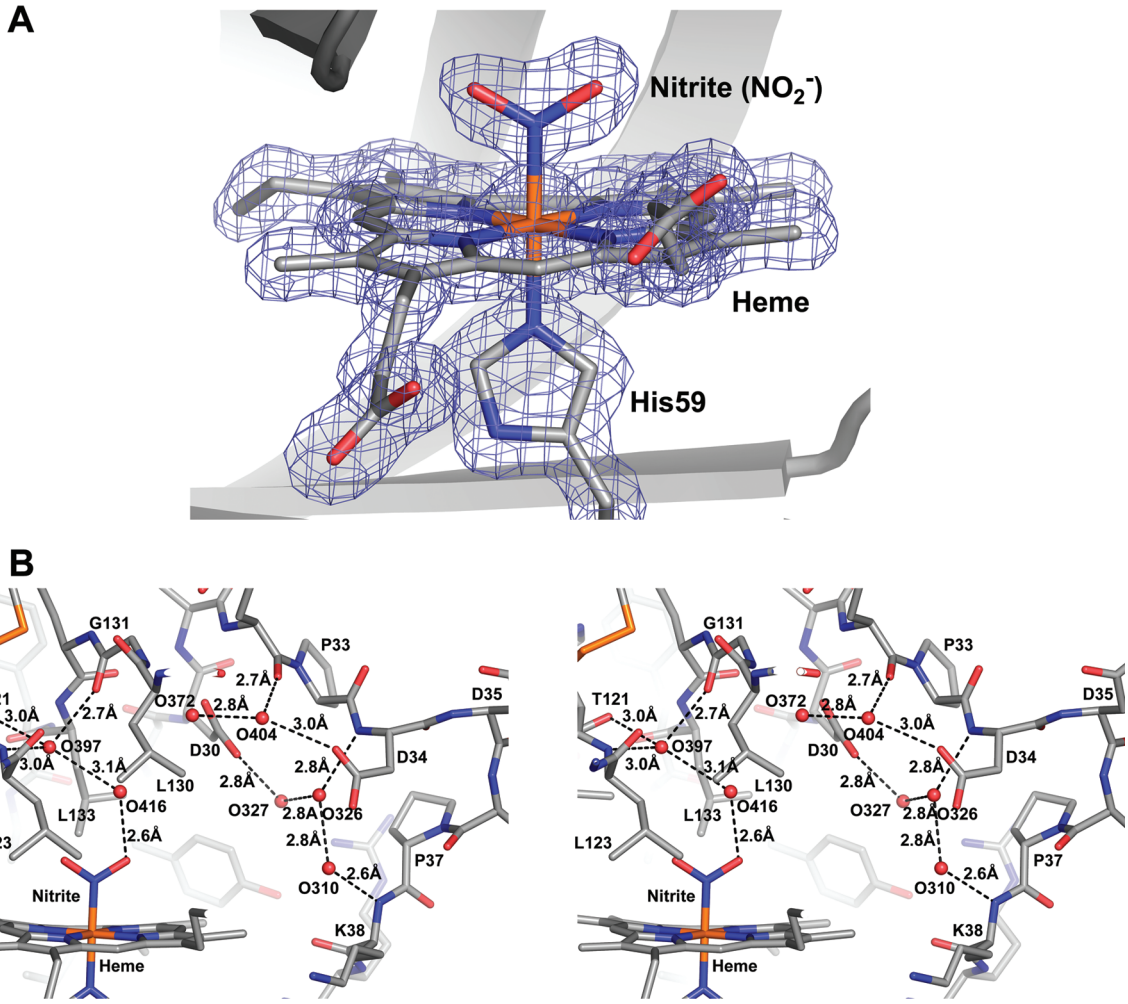

FIGURE 6: X-ray crystal structure of NP4 from *R. prolixus* soaked with NO_2^- at pH 7.4 at 1.4 Å resolution. (A) The $2F_o - F_c$ electron density map of the heme cofactor and its ligands is shown. On the upper heme plane, a nitrite molecule fits well into the electron density contour. (B) Stereoview of a stick representation of NP4 near the heme pocket and the A−B loop. The possible hydrogen bonds via water molecules (red spheres) are represented by the dashed lines.

KNO_2 was adjusted according to the EPR and RR studies to minimize the formation of NO before the crystals were frozen.

The crystals diffracted to 1.4 Å resolution (Table 4), and the structure was determined by the molecular replacement method based on the model of the already published NP4 structures. The overall fold (see Figure S3 of the Supporting Information) was very similar to the established NP4 structures with significant differences only in the A−B loop region (see below). Figure 6A displays the electron density map of the heme cofactor and the ligands. On the upper side of the cofactor, electron density is observed that can be modeled well by an η^1-N coordinated NO_2^-. The Fe−$N_{nitrite}$ and Fe−N^{τ}_{His59} distances are 1.96 and 2.01 Å, respectively. The imidazole$_{His59}$ plane and the NO_2^- plane are parallel (2° deviation) and oriented along the $C^{meso\text{-}\beta}$–$C^{meso\text{-}\delta}$ axis, i.e., 37° and 39°, respectively, oriented to the closest N_p−Fe−N_p axis. The angle between the ligand planes is nearly straight [$\angle(N_{nitrite}\text{−Fe−}N^{\tau}_{His59}) = 179°$]. A second NO_2^- is bound to Asp68 and Lys88, a location far from the cofactor and, therefore, probably simply a consequence of the high NO_2^- concentration under the crystallization conditions (Figure S4 of the Supporting Information).

The pH-dependent change in the flexibility of the two loops termed A−B and G−H in front of the heme cofactor is a major structural determinant of the NO delivery process of NP4 (*43*, *45*, *46*). Comparison with other NP4 structures revealed that NP4[NO_2^-] constitutes an open A−B loop conformation that is depicted in Figure 6B. Like with all NP4 structures, the A−B loop shows a high degree of flexibility (see Figure S3 of the Supporting Information) but is still well-defined as can be seen from the electron density map in Figure S5 of the Supporting Information. Furthermore, the crystal symmetry and the crystal packing did not deviate when the crystals were soaked with NO_2^- (Figure S3 of the Supporting Information) so that A−B loop rearrangement can be identifed as not being a crystallographic artifact.

The A−B loop in this case reveals a strong backbone rearrangement, i.e., between Pro33 and Tyr40; as a consequence of this rearrangement, the side chain of Asp35 moves out of the heme pocket where Asp34 moves toward the heme pocket, which further affects the positions of waters in the proximity of the heme (Figure 6B). Overall, where the A−B loop in the majority of the NP4 X-ray structures appears in a closed conformation, in some of the structures an open loop conformation was obtained. However, although the backbone of NP4[NO_2^-] compares better with the open A−B loop, this conformation is unique among all the NP4 structures (see Figure S6 of the Supporting Information). Superposition of the structures of NP4[NO_2^-] and NP4[NH_3] (PDB entry 1X8P) (*43*) shows that one of the NO_2^-

oxygens is oriented toward the methyl carbons of Val36 with an $O_{nitrite}-C_{Val36}$ distance of 3.8 Å. Thus, we can conclude that electrostatic repulsion may trigger the conformational change of the A−B loop upon NO_2^- binding (Figure S7 of the Supporting Information). At present, NO_2^- is the only structure of NP4 with a charged iron ligand. In contrast, the more hydrophobic ligands NO and imidazole cause the A−B loop to close, even at low pH (*43*, *47*). Thus, Val36 seems to play a major role in the sensing of the ligand and the response of the A−B loop conformation.

DISCUSSION

Spectral changes in UV−vis absorption spectroscopy upon binding of NO_2^- to NP4 and NP7 are small, although the eye detects a significant color change. Small absorption differences are also observed in the case of other ferriheme proteins, namely metMb, metHb (*16*, *48*), and ferriheme cd_1 nitrite reductase (NiR) (*49*). The increase in the magnitude of the α- and β-bands at ~570 and ~530 nm, respectively (Figure 1), is a strong indication for the formation of a Fe^{III} low-spin complex, which is confirmed by RR and EPR spectroscopy (Figures 4 and 5). The change in absorption was used to follow the binding of NO_2^- to the proteins (Figure 2). It is important to note that the formation of the initial complex is faster than the total reaction represented in Scheme 1 (*8*). However, UV−vis absorption spectroscopy is not unambiguous for the identification of the product because the decrease in the Soret absorption together with the increase in the magnitude of the α- and β-bands are also features of the formation of NP4/7[NO]. RR and EPR spectroscopy confirm that within the time of the kinetic measurements no significant amount of $\{FeNO\}^6$ is formed so that studies of the initial complex are possible.

In principle, the NO_2^- anion can coordinate in three different orientations to the metal center of a porphyrin, i.e., the η^1-N bound nitro form and in the η^1-O and η^2-O bound nitrito forms (*50*, *51*). In synthetic iron porphyrins, the N-bound form was found to be significantly more stable (*42*), although the five-coordinate complex of [Fe(*meso*-tetra-*p*-tolylporphyrinato)-(η^1-ONO)] was obtained (*52*). However, upon addition of a sixth coordinating ligand, the η^1-O liganded complex readily converted into the η^1-N species (*52*, *53*). An examination of the few X-ray structures of ferriheme proteins in complex with NO_2^- reveals that the η^1-N complex appears in most cases, i.e., *Thiosphera panthotropha* NiR (*54*), *Thioalkalivibria nitratireducens* NiR (*55*), *Wollinella succinogenes* NiR (*56*), and *E. coli* sulfite reductase hemoprotein (SiRHP) (*57*). Of these examples, only *T. panthotropha* NiR has a His *trans* to NO_2^-, but a hydroheme (heme d_1) is located in the active site (*54*). Where, in contrast, the two other NiR forms have a heme *c*, the iron in these cases is coordinated by Lys (*55*, *56*). Finally, SiHRP also contains a hydroheme (siroheme), but the iron coordination is performed by a very unusual $Cys-[Fe_4S_4]_{cluster}$ ligand (*57*). Thus, it appears that this is the first report of an η^1-N coordinated NO_2^- complex of a fully unsaturated heme inside a protein coordinated by a His residue.

Like NPs, Mb and Hb coordinate a heme *b* via a His residue. However, for both proteins it has been confirmed by X-ray crystallography that the proteins stabilize the $Fe^{III}-\eta^1$-ONO^- complex (*10*, *58*), which is currently the only example of a stable porphyrin (N-base$-Fe^{III}-\eta^1$-ONO^-). A recent examination of site-specific mutants in combination with X-ray crystallography experiments revealed that the NO_2^- orientation in metMb is dictated by the surrounding residues (*11*). The X-ray crystallographic analysis of NP4[NO_2^-] clearly shows the formation of an η^1-N bound NO_2^-. The fact that ferrihemes in general prefer the η^1-N coordination principally suggests the formation of NP[$Fe^{III}-\eta^1$-NO_2^-]. This is further supported by the recent finding that mutation of the distal pocket residue His64 to Val in Mb disrupts the formation of the nitrito complex where insertion of another H bonding residue, i.e., Mb(H64V,V67R), restored the formation of Mb[$Fe^{III}-\eta^1$-ONO^-]. It was concluded that the presence of an H bonding side chain in the heme pocket is crucial for this particular NO_2^- orientation (*11*). However, the heme pocket of NPs is characterized by the presence of numerous carboxylate residues concomitant with a lack of positively charged side chains (*29*), so that a stabilization of a nitrito ligand is not to be expected in NPs.

cw-EPR spectroscopy of NP4/7[NO_2^-] reveals the formation of a low-spin complex ($S = {}^1/_2$). RR spectra further indicate the presence of a six-coordinate complex, i.e., the His59/60 on. This cannot be established from the EPR spectra per se because five-coordinate nitro complexes usually also exhibit a low-spin complex (*59*, *60*). The EPR parameters of two well-characterized model hemes, [Fe(TpivPP)(η^1-NO_2)(py)] and [Fe(TpivPP)(η^1-NO_2)-(ImH)], are included in Table 3 (*42*). Like the proteins discussed here, these compounds exhibit π-donor base ligands *trans* to NO_2^-. Calculation of the rhombicity parameter V/Δ assuming the conventional coordination system, which suggests that the principle magnetic axis (assigned to *z*) is along the heme normal (i.e., $g_z = g_1$, $g_y = g_2$, and $g_x = g_3$), results in values exciding the $V/\Delta = {}^2/_3$ threshold (*40*, *42*). This might suggest a change in the direction of the principal magnetic axis where others ascribe this large rhombicity to the good π-acceptor and σ-donor abilities of the η^1-NO_2^- ligand (*59*). In agreement with the latter, complexes [Fe(TpivPP)(η^1-NO_2)$_2$]$^-$ and [Fe(TpivPP)(η^1-NO_2)(SC_6F_4H)]$^-$ exhibited V/Δ values of 1.34 (*61*) and 1.27 (*62*), respectively. Consequently, η^1-ONO^-, which is considered a good σ-donor but a much poorer π-acceptor (*63*) in the structurally well-defined compounds metMb[η^1-ONO^-] and metHb[η^1-ONO^-], exhibits a much smaller rhombicity (Table 3). The large rhombicity observed for NP4 and NP7 strongly supports the formation of a nitro complex.

Most of the proteins reveal two low-spin components in their EPR spectra (Figure 5 and Table 3). Where the two sets of *g* values of NP7 are rather similar, the divergence between the two sets of NP4 forms is very large; i.e., the spectrum of $LS2^{NP4}$ resembles a "large g_{max}" type of spectrum. It was speculated earlier that in the case of metHb[η^1-ONO^-] the two low-spin species may correspond to either (i) the presence of two different heme centers in Hb originating from the heterotetrameric $\alpha_2\beta_2$ tertiary structure or (ii) the concomitant appearance of a nitro and a nitrito complex (*31*). However, (i) two low-spin species are also observed for many monomeric proteins, and (ii) there is no support by the X-ray crystal structures of metHb[η^1-ONO^-] (*10*) and metMb[η^1-ONO^-] (*58*). Consequently, the origin of the two electronically different species requires an explanation.

Because EPR spectroscopy is primarily sensitive to the ligand orientation rather than the nature of the ligand, which was extensively shown for bis-imidazole-coordinated hemes (*41*, *64*), the two sets of low-spin signals likely reflect two distinct orientations of NO_2^- bound to the heme iron; thus, $LS2^{NP7}$, $LS3^{NP7}$, and $LS3^{NP4}$ reflect a close to parallel ligand plane orientation which is seen in the NP4[NO_2^-] structure. In

contrast, the structurally well-defined model complexes [Fe(TpivPP)(η^1-NO_2)(py)] and [Fe(TpivPP)(η^1-NO_2)(ImH)] exhibit a more perpendicular ligand orientation ($\Delta\phi$ = 77° and 69°, respectively) (*42*) which results in larger g_{max} values (*41*). Notably, the alignment of NO_2^- with respect to the heme plane is comparable, i.e., along those *meso* carbons that orient out of the normal heme plane toward NO_2^- of these nonplanar hemes, and the Fe−$N_{imidazole/py}$ and Fe−$N_{nitrite}$ distances are nearly identical. In contrast, the "large g_{max}" type of spectrum $LS2^{NP4}$ can be interpreted in terms of a perpendicular ligand plane orientation. Recently, the pH dependence of the **A**:**B**[4] ratio in NP2[ImH] was examined in detail by NMR spectroscopy (pH* 7.0 to 4.0)[5] (*65*, *66*). During this study, besides the well-established ^{1}H resonances originating from **A** and **B**, a novel set of resonances appeared with a decreasing pH, and the corresponding species was designated **B**′. **B**′, which is in slow chemical exchange with **B**, so that for **B**′ ⇄ **B**, k_1 = 8.0 s^{-1} and k_{-1} = 1.0 s^{-1} at pH* 5.5 and 30 °C, was further characterized to have the ImH plane ligand orientation nearly perpendicular to that of **B** (*66*). In accordance with these observations, the ImH experiments clearly indicate that the protein provides enough steric freedom for a three-atom V-shaped molecule to rotate in a fashion similar to that of ImH. Although **B**′ was not yet observed in X-ray crystallography, comparison of the crystal structures available for NP4[ImH] (pH 5.6) (*47*) and NP2[ImH] (pH 6.5) (*67*) reasonably explains the behavior (*66*). However, this is a very simple explanation that requires further careful analysis for a detailed understanding of the electronics of the system.

The kinetic parameters of the reaction depicted in Scheme 2 are summarized in Table 1 and are compared to the data obtained for metMb and metHb. It is obvious that the rate of binding (k_1) to NP4/7 is significantly lower compared to those of metMb and metHb. Interestingly, the rate of the release (k_{-1}) is also significantly slower, so that K_{eq} is similar to the globins. Sufficient fitting of the kinetic traces is achieved only if a double exponential is applied (Figure 2A,B). However, the linear behavior of the plot of k_{obs} versus NO_2^- concentration suggests the existence of independent fast and slow processes for both proteins. A similar model was used in the case of metHb + NO_2^- which can be explained with the heterotetrameric $\alpha_2\beta_2$ tertiary structure, and hence the appearance of two distinct heme centers (*16*). Where this interpretation does certainly not apply for NP4 and NP7, a possible explanation may be the presence of two NO_2^- binding modes, i.e., in linear and perpendicular orientation relative to His59/60. On the other hand, NO_2^- was obtained in the crystals only in the parallel orientation, which, on the basis of EPR spectroscopy, is favored in NP4 (Table 3), yet this may be due to the crystallization conditions. Currently, the origin of the two processes cannot be sufficiently explained, and further experimental work is required.

In summary, X-ray crystallography and spectroscopic data strongly reveal the formation of the common η^1-N bound nitro complexes in the case of the lipocalin type heme proteins NP4 and NP7 rather than the unusual η^1-O nitrito form obtained with the globin type metHb and metMb. This may, at least in part, account for the different reactivities observed between the two classes of proteins. Moreover, differences from the globins are also seen in the much slower association rates. On the other hand, the absence of the nitrite disproportionation reaction with other ferrihemes at neutral pH infers that this is a specific feature of nitrophorin structure. Moreover, the equilibration constants for NO_2^- ligand binding, although very small, are comparable to those of the globins. In the case of Mb and Hb, NO_2^- is widely accepted as a physiological relevant substrate (*14*, *68*). Because NPs in principle have the same "working environment", i.e., the blood, this strengthens the argument that NPs have the potential to use NO_2^- as a substrate in vivo as well.

[4]Because of the substituent arrangement of the protoporphyrin IX macrocycle, the heme *b* cofactor binds to the asymmetric environment of a protein's heme pocket in two different orientations, **A** and **B**. This phenomenon is often termed the "heme rotational disorder". For the determination of the orientation, the protoporphyrin IX ring is examined on top of the side opposite the coordinating His. If the pyrrole ring counting follows a clockwise order, then the orientation is termed **A**, otherwise **B**.

[5]The pH was not corrected for the D_2O used as the solvent.

ACKNOWLEDGMENT

We are grateful for the technical assistance of Johanna Taing, Jan Hanis, Marion Stapper, Gudrun Klihm, and Frank Reikowski at our institute. We further thank the staff of beamline BL14.2 at BESSYII for their assistance during the data collection. We thank Prof. F. Ann Walker (Department of Chemistry and Biochemistry, University of Arizona, Tucson, AZ) for the expression vectors.

SUPPORTING INFORMATION AVAILABLE

Kinetic traces of formation of the NP7[NO] complex (Figure S1), kinetic trace and correction of the NP7[NO_2^-] formation (Figure S2), overview of the total X-ray structure of NP4[NO_2^-] (Figure S3), binding site of the second NO_2^- (Figure S4), representation of the electron density of the A−B loop region in the X-ray structure of NP4[NO_2^-] (Figure S5), superposition of backbone structures of the A−B loop region of all NP4 structures available from Protein Data Bank (Figure S6), and superposition of the A−B loop region side chains of NP4[NO_2^-] with two other NP4 structures (Figure S7). This material is available free of charge via the Internet at http://pubs.acs.org.

REFERENCES

1. Walker, F. A., and Montfort, W. R. (2001) The nitric oxide-releasing heme proteins from the saliva of the blood-sucking insect *Rhodnius prolixus*. In Advances in Inorganic Chemistry, Vol. *51* pp 295−358, Academic Press, San Diego.
2. Walker, F. A. (2005) Nitric oxide interaction with insect nitrophorins and thoughts on the electron configuration of the $\{FeNO\}^6$ complex. *J. Inorg. Biochem. 99*, 216–236.
3. Andersen, J. F., Gudderra, N. P., Francischetti, I. M. B., Valenzuela, J. G., and Ribeiro, J. M. C. (2004) Recognition of anionic phospholipid membranes by an antihemostatic protein from a blood-feeding insect. *Biochemistry 43*, 6987–6994.
4. Knipp, M., Zhang, H., Berry, R. E., and Walker, F. A. (2007) Overexpression in *Escherichia coli* and functional reconstitution of the liposome binding ferriheme protein nitrophorin 7 from the blood sucking bug *Rhodnius prolixus*. *Protein Expression Purif. 54*, 183–191.
5. Knipp, M., Yang, F., Berry, R. E., Zhang, H., Shokhirev, M. N., and Walker, F. A. (2007) Spectroscopic and functional characterization of nitrophorin 7 from the blood-feeding insect *Rhodnius prolixus* reveals an important role of its isoform-specific N-terminus for proper protein function. *Biochemistry 46*, 13254–13268.
6. Andersen, J. F., Weichsel, A., Balfour, C. A., Champagne, D. E., and Montfort, W. R. (1998) The crystal structure of nitrophorin 4 at 1.5 Å resolution: Transport of nitric oxide by a lipocalin-based heme protein. *Structure 6*, 1315–1327.
7. Bianchetti, C. M., Blouin, G. C., Bitto, E., Olson, J. S., and Phillips, G. N., Jr. (2010) The structure and NO binding properties of the nitrophorin-like heme-binding protein from *Arabidopsis thaliana* gene locus At1g79260.1. *Proteins 78*, 917–931.
8. He, C., and Knipp, M. (2009) Formation of nitric oxide from nitrite by the ferriheme *b* protein nitrophorin 7. *J. Am. Chem. Soc. 131*, 12042–12043.

9. Samouilov, A., Kuppusamy, P., and Zweier, J. L. (1998) Evaluation of the magnitude and rate of nitric oxide production from nitrite in biological systems. *Arch. Biochem. Biophys. 375*, 1–7.
10. Yi, J., Safo, M. K., and Richter-Addo, G. B. (2008) The nitrite anion binds to human hemoglobin via the uncommon *O*-nitrito mode. *Biochemistry 47*, 8247–8249.
11. Yi, J., Heinecke, J., Tan, H., Ford, P. C., and Richter-Addo, G. B. (2009) The distal pocket histidine residue in horse heart myoglobin directs the O-binding mode of nitrite to the heme iron. *J. Am. Chem. Soc. 131*, 18119–18128.
12. Basu, S., Grubina, R., Huang, J., Conradie, J., Huang, Z., Jeffers, A., Jiang, A., He, X., Azarov, I., Seibert, R., Mehta, A., Patel, R., King, B. S., Hogg, N., Ghosh, A., Gladwin, M. T., and Kim-Shapiro, D. B. (2007) Cataclytic generation of N_2O_3 by the concerted nitrite reductase and anhydrase activity of hemoglobin. *Nat. Chem. Biol. 3*, 785–794.
13. Gladwin, M. T., Schechter, A. N., Kim-Shapiro, D. B., Patel, R. P., Hogg, N., Shiva, S., Cannon, R. O., III, Kelm, M., Wink, D. A., Espey, M. G., Oldfield, E. H., Pluta, R. M., Freeman, B. A., Lancaster, J. R., Jr., Feelisch, M., and Lundberg, J. O. (2005) The emerging biology of the nitrite anion. *Nat. Chem. Biol. 1*, 308–314.
14. Gladwin, M. T., Grubina, R., and Doyle, M. P. (2009) The new chemical biology of nitrite reactions with hemoglobin: R-state catalysis, oxidative denitrosylation, and nitrite reductase/anhydrase. *Acc. Chem. Res. 42*, 157–167.
15. Perissinotti, L. L., Marti, M. A., Doctorovich, F., Luque, F. J., and Estrin, D. A. (2008) A microscopic study of the deoxyhemoglobin-catalyzed generation of nitric oxide from nitrite anion. *Biochemistry 47*, 9793–9802.
16. Wanat, A., Gdula-Argasińska, J., Rutkowska-Żbik, D., Witko, M., Stochel, G., and van Eldik, R. (2002) Nitrite binding to metmyoglobin and methemoglobin in comparison to nitric oxide binding. *J. Biol. Inorg. Chem. 7*, 165–176.
17. Strickler, S. J., and Kasha, M. (1963) Solvent effects on the electronic absorption spectrum of nitrite ion. *J. Am. Chem. Soc. 85*, 2899–2901.
18. Berry, R. E., Shokhireva, T. K., Filippov, I., Shokhirev, M. N., Zhang, H., and Walker, F. A. (2007) The effect of the N-terminus on heme cavity structure, ligand equilibrium and rate constants and reduction potentials of nitrophorin 2 from *Rhodnius prolixus*. *Biochemistry 46*, 6830–6843.
19. Maes, E. M., Roberts, S. A., Weichsel, A., and Montfort, W. R. (2005) Ultrahigh resolution structures of nitrophorin 4: Heme distortion in ferrous CO and NO complexes. *Biochemistry 44*, 12690–12699.
20. Hagen, W. R. (2009) Biomolecular EPR Spectroscopy, 1st ed., CRC Press, Boca Raton, FL.
21. Kabsch, W. (1993) Automatic processing of rotation diffraction data from crystals of initially unknown symmetry and cell constants. *J. Appl. Crystallogr. 26*, 795–800.
22. Collaborative Computational Project, Number 4 (1994) The *CCP*4 suite: Programs for protein crystallography. *Acta Crystallogr. D50*, 760–763.
23. Emsley, P., and Cowtan, K. (2004) Coot: Model-building tools for molecular graphics. *Acta Crystallogr. D60*, 2126–2132.
24. Lovell, S. C., Davis, I. W., Arendall, W. B., III, de Bakker, P. I. W., Word, J. M., Prisant, M. G., Richardson, J. S., and Richardson, D. C. (2003) Structure validation by Cα geometry: ϕ, ψ, and Cβ deviation. *Proteins: Struct., Funct., Genet. 50*, 437–450.
25. Andersen, J. F., Ding, X. D., Balfour, C., Shokhireva, T. K., Champagne, D. E., Walker, F. A., and Montfort, W. R. (2000) Kinetics and equilibria in ligand binding by nitrophorins 1−4: Evidence for stabilization of a nitric oxide-ferriheme complex through a ligand-induced conformational trap. *Biochemistry 39*, 10118–10131.
26. Rodkey, F. L. (1976) A mechanism for the conversion of oxyhemoglobin to methemoglobin by nitrite. *Clin. Chem. 22*, 1986–1990.
27. Smith, R. P. (1967) The nitrite methemoglobin complex: Its significance in methemoglobin analyses and its possible role in methemoglobinemia. *Biochem. Pharmacol. 16*, 1655–1664.
28. Kaneko, Y., Yuda, M., Iio, T., Murase, T., and Chinzei, Y. (1999) Kinetic analysis on nitric oxide binding of recombinant Prolixin-S, a nitric oxide transport protein from the bloodsucking bug. *Rhodnius prolixus*. *Biochim. Biophys. Acta 1431*, 492–499.
29. Berry, R. E., Shokhirev, M. N., Ho, A. Y. W., Yang, F., Shokhireva, T. K., Zhang, H., Weichsel, A., Montfort, W. R., and Walker, F. A. (2009) Effect of mutation of carboxyl side-cahin amino acids near the heme on the midpoint potentials and ligand binding constants of nitrophorin 2 and its NO, histamine, and imidazole complexes. *J. Am. Chem. Soc. 131*, 2313–2327.
30. Schwab, D. E., Stamler, J. S., and Singel, D. J. (2009) Nitrite-methemoglobin inadequate for hypoxic vasodilation. *Nat. Chem. Biol. 5*, 366.
31. Goetz, B. I., Shields, H. W., Basu, S., Wang, P., King, S. B., Hogg, N., Gladwin, M. T., and Kim-Shapiro, D. B. (2009) An electron paramagnetic resonance study of the affinity of nitrite for methemoglobin. *Nitric Oxide 22*, 149–154.
32. Maes, E. M., Walker, F. A., Montfort, W. R., and Czernuszewicz, R. S. (2001) Resonance Raman spectroscopic study of nitrophorin 1, a nitric oxide-binding heme protein from *Rhodnius prolixus*, and its nitrosyl and cyano adducts. *J. Am. Chem. Soc. 123*, 1164–1172.
33. Kincaid, J. R. (2000) Resonance Raman spectra of heme proteins and model compounds. In The Porphyrin Handbook (Kadish, K. M., Smith, K. M., and Guilard, R., Eds.) Vol. *7*, pp 225−291, Academic Press, San Diego.
34. Spiro, T. G., Stong, J. D., and Stein, P. (1979) Porphyrin core expansion and doming in heme proteins. New evidence from resonance Raman spectra of six-coordinate high-spin iron(III) hemes. *J. Am. Chem. Soc. 101*, 2648–2655.
35. Zareba, A. A. (2006) Resonance Raman spectroscopic characterization of nitrophorins from *Rhodnius prolixus* and *Cimex lectularius*. Ph.D. Thesis, Department of Chemistry, University of Houston, Houston.
36. Choi, S., Spiro, T. G., Langry, K. C., Smith, K. M., Budd, D. L., and La Mar, G. N. (1982) Structural correlations and vinyl influences in resonance Raman spectra of protoheme complexes and proteins. *J. Am. Chem. Soc. 104*, 4345–4351.
37. Ikeda-Saito, M., Hori, H., Andersson, L. A., Prince, R. C., Pickering, I. J., George, G. N., Sanders, C. R., II, Lutz, R. S., McKelvey, E. J., and Mattera, R. (1992) Coordination structure of the ferric heme iron in engineered distal histidine myoglobin mutants. *J. Biol. Chem. 267*, 22843–22852.
38. Taylor, C. P. S. (1977) The EPR of low spin heme complexes. Relation of the t_{2g} hole model to the directional properties of the *g* tensor, and a new method for calculating the ligand field parameters. *Biochim. Biophys. Acta 491*, 137–149.
39. Zoppellaro, G., Bren, K. L., Ensign, A. A., Herbitz, E., Kaur, R., Hersleth, H.-P., Ryde, U., Hederstedt, L., and Andersson, R. K. (2009) Studies of ferric heme proteins with highly anisotropic/highly axial low spin ($S = 1/2$) electron paramagnetic resonance signals with bis-histidine and histidine-methionine axial iron coordination. *Biopolymers 91*, 1064–1082.
40. Palmer, G. (2000) Electron Paramagnetic Resonance of Metalloproteins. In *Physical Methods in Bioinroganic Chemistry* (Que, L., Ed.) pp 121−186, University Science Books, Sausalito, CA.
41. Walker, F. A. (2004) Models of the bis-histidine-ligated electron-transferring cytochromes. Comparative geometric and electronic structure of low-spin ferro- and ferrihemes. *Chem. Rev. 104*, 589–615.
42. Nasri, H., Wang, Y., Huynh, B. H., Walker, F. A., and Scheidt, W. R. (1991) Reactions of bis(nitro)(α,α,α,α-tetrakis(*o*-pivalamidophenyl)-porphinato)ferrat(III) with pyridine and imidazole. EPR and Mössbauer spectra and molecular structures of the mixed-ligand species. *Inorg. Chem. 30*, 1483–1489.
43. Kondrashov, D. A., Roberts, S. A., Weichsel, A., and Montfort, W. R. (2004) Protein functional cycle viewed at atomic resolution: Conformational change and mobility in nitrophorin 4 as a function of pH and NO binding. *Biochemistry 43*, 13637–13647.
44. Schmidt, M., Achterhold, K., Prusakov, V., and Parak, F. G. (2009) Protein dynamics of a β-sheet protein. *Eur. Biophys. J. 38*, 687–700.
45. Maes, E. M., Weichsel, A., Andersen, J. F., Shepley, D., and Montfort, W. R. (2004) Role of binding site loops in controlling nitric oxide release: Structure and kinetics of mutant forms of nitrophorin 4. *Biochemistry 43*, 6679–6690.
46. Swails, J. M., Meng, Y., Walker, F. A., Martí, M. A., Estrin, D. A., and Roitberg, A. E. (2009) pH-dependent mechanism of nitric oxide release in nitrophorin 2 and 4. *J. Phys. Chem. B 113*, 1192–1201.
47. Roberts, S. A., Weichsel, A., Qiu, Y., Shelnutt, J. A., Walker, F. A., and Montfort, W. R. (2001) Ligand-induced heme ruffling and bent NO geometry in ultra-high-resolution structures of nitrophorin 4. *Biochemistry 40*, 11327–11337.
48. Young, L. J., and Siegel, L. M. (1988) On the reaction of ferric heme proteins with nitrite and sulfite. *Biochemistry 27*, 2790–2800.
49. van Wonderen, J. H., Knight, C., Oganesyan, V. S., George, S. J., Zumpft, W. G., and Cheesman, M. R. (2007) Activation of the cytochrome cd_1 nitrite reductase from *Paracoccus pantotrophus*: Reaction of oxidized enzyme with substrate drives a ligand switch at heme *c*. *J. Biol. Chem. 282*, 28207–28215.
50. Wyllie, G. R. A., and Scheidt, W. R. (2002) Solid-state structures of metalloporphyrin NO_x compounds. *Chem. Rev. 102*, 1067–1089.

51. Heinecke, J., and Ford, P. C. (2010) Mechanistic studies of nitrite reactions with metalloproteins and models relevant to mammalian physiology. *Coord. Chem. Rev. 254*, 235–247.
52. Kurtikyan, T. S., and Ford, P. C. (2006) Reactions of nitrogen oxides with heme models: Spectral charcterization of an elusive five-coordinate Fe^{III}(porphyrin) nitrtito intermediate. *Angew. Chem., Int. Ed. 45*, 492–496.
53. Kurtikyan, T. S., Hovhannisyan, A. A., Gulyan, G. M., and Ford, P. C. (2007) Interaction of nitrogen bases with iron-porphyrin nitrito complexes Fe(Por)(ONO) in sublimed solids. *Inorg. Chem. 46*, 7024–7031.
54. Williams, P. A., Fülöp, V., Garman, E. F., Saunders, N. F. W., Ferguson, S. J., and Hajdu, J. (1997) Haem-ligand switching during catalysis in crystals of a nitrogen-cycle enzyme. *Nature 389*, 406–412.
55. Polyakov, K. M., Boyko, K. M., Tikhonova, T. V., Slutsky, A., Antipov, A. N., Zvyagilskaya, R. A., Popov, A. N., Bourenkov, G. P., Lamzin, V. S., and Popov, V. O. (2009) High-resolution structural analysis of a novel octaheme cytochrome *c* nitrite reductase from the haloalkaliphilic bacterium *Thioalkalivibrio nitratireducens*. *J. Mol. Biol. 389*, 846–862.
56. Einsle, O., Messerschmidt, A., Huber, R., Kroneck, P. M. H., and Neese, F. (2002) Mechanism of the six-electron reduction of nitrite to ammonia by cytochrome *c* nitrite reductase. *J. Am. Chem. Soc. 124*, 11737–11745.
57. Crane, B. R., Siegel, L. M., and Getzoff, E. D. (1997) Probing the catalytic mechanism of sulfite reductase by X-ray crystallography: Structures of the *Escherichia coli* hemoprotein in complex with substrates, inhibitors, intermediates, and products. *Biochemistry 36*, 12120–12137.
58. Copeland, D. N., Soares, A. S., West, A. H., and Richter-Addo, G. B. (2006) Crystal structures of the nitrite and nitric oxide complexes of horse heart myoglobin. *J. Inorg. Biochem. 100*, 1413–1425.
59. Conradie, J., and Ghosh, A. (2006) Iron(III)-nitro porphyrins: Theoretical exploration of a unique class of reactive molecules. *Inorg. Chem. 45*, 4902–4909.
60. Nasri, H., Wang, Y., Huynh, B. H., and Scheidt, W. R. (1991) Nitrite-bound five-coordinate low-spin iron(II) model complex for the prosthetic group of nitrite reductase with an unusually large quadrupole splitting. Synthesis, Mössbauer properties, and molecular structure of the complex (nitro)(α,α,α,α-tetrakis(*o*-pivalamidophenyl)porphinato)-iron(II). *J. Am. Chem. Soc. 113*, 717–719.
61. Nasri, H., Goodwin, J. A., and Scheidt, W. R. (1990) Use of protected binding sites for nitrite binding in iron(III) porphyrinates. Crystal structure of the bis(nitro)(α,α,α,α-tetrakis(*o*-pivalamidophenyl)-porphinato)iron(III) anion. *Inorg. Chem. 29*, 185–191.
62. Nasri, H., Haller, K. J., Wang, Y., Huynh, B. H., and Scheidt, W. R. (1992) Reactions of bis(nitro)[α,α,α,α-*meso*-tetrakis(*o*-pivalamidophenyl)porphinato]iron(III) with 2,3,5,6-tetraflurothiophenol and 2,3,5,6-tetrafluorothiophenolate. EPR and Mössbauer spectra and molecular structures. *Inorg. Chem. 31*, 3459–3467.
63. Hitchman, M. A., and Rowbottom, G. L. (1982) Transition metal nitrite complexes. *Coord. Chem. Rev. 42*, 55–132.
64. Walker, F. A. (1999) Magnetic spectroscopy (EPR, ESEEM, Mössbauer, MCD and NMR) studies of low-spin ferriheme centers and their corresponding heme proteins. *Coord. Chem. Rev. 185−186*, 471–534.
65. Yang, F., Zhang, H., and Knipp, M. (2009) A one-residue switch reverses the orientation of a heme *b* cofactor. Investigations on the ferriheme NO transporters nitrophorin 2 and 7 from the blood-feeding insect *Rhodnius prolixus*. *Biochemistry 48*, 235–241.
66. Yang, F., Knipp, M., Shokhireva, T. K., Berry, R. E., Zhang, H., and Walker, F. A. (2009) A ^{1}H and ^{13}C NMR spectroscopic study of the ferriheme resonances of three low-spin complexes of wild-type nitrophorin 2 and nitrophorin2(V24E) as a function of pH. *J. Biol. Inorg. Chem. 14*, 1077–1095.
67. Andersen, J. F., and Montfort, W. R. (2000) The crystal structure of nitrophorin 2. A trifunctional antihemostatic protein from the saliva of *Rhodnius prolixus*. *J. Biol. Chem. 275*, 30496–30503.
68. Shiva, S., Huang, Z., Grubina, R., Sun, J., Ringwood, L. A., MacArthur, P. H., Xu, X., Murphy, E., Darley-Usmar, V. M., and Gladwin, M. T. (2007) Deoxymyoglobin is a nitrite reductase that generates nitric oxide and regulates mitochondrial respiration. *Circ. Res. 100*, 654–661.
69. Gibson, Q. H., Parkhurst, L. J., and Geraci, G. (1969) The reaction of methemoglobin with some ligands. *J. Biol. Chem. 244*, 4668–4676.
70. Hagedoorn, P. L., de Geus, D. C., and Hagen, W. R. (2002) Spectroscopic characterization and ligand-binding properties of chlorite dismutase from the chlorate respiring bacterial strain GR-1. *Eur. J. Biochem. 269*, 4905–4911.